Deep-Sea Research I 116 (2016) 118–126

Contents lists available at ScienceDirect

Deep-Sea Research I

journal homepage: www.elsevier.com/locate/dsri

Geochemical characteristics of sinking particles in the Tonga arc hydrothermal vent field, southwestern Pacific

Hyung Jeek Kim [a], Jonguk Kim [a], Sang Joon Pak [a], Se-Jong Ju [a], Chan Min Yoo [a], Hyun Sub Kim [a], Kyeong Yong Lee [a], Jeomshik Hwang [b,*]

[a] Deep-sea Resources Research Center, Korea Institute of Ocean Science & Technology, Ansan, South Korea
[b] School of Earth and Environmental Sciences/Research Institute of Oceanography, Seoul National University, Seoul, South Korea

ARTICLE INFO

Article history:
Received 25 January 2016
Received in revised form
25 March 2016
Accepted 1 July 2016
Available online 20 August 2016

Keywords:
Hydrothermal vent systems
Tonga arc
Sinking particle flux
Trace metals
Sediment trap

ABSTRACT

Studies of sinking particles associated with hydrothermal vent fluids may help us to quantify mass transformation processes between hydrothermal vent plumes and deposits. Such studies may also help us understand how various types of hydrothermal systems influence particle flux and composition. However, the nature of particle precipitation out of hydrothermal vent plumes in the volcanic arcs of convergent plate boundaries has not been well studied, nor have the characteristics of such particles been compared with the characteristics of sinking particles at divergent boundaries. We examined sinking particles collected by sediment traps for about 10 days at two sites, each within 200 m of identified hydrothermal vents in the south Tonga arc of the southwestern Pacific. The total mass flux was several-fold higher than in the non-hydrothermal southwest tropical Pacific. The contribution of non-biogenic materials was dominant (over 72%) and the contribution of metals such as Fe, Mn, Cu, and Zn was very high compared to their average levels in the upper continental crust. The particle flux and composition indicate that hydrothermal authigenic particles are the dominant source of the collected sinking particles. Overall, our elemental ratios are similar to observations of particles at the divergent plate boundary in the East Pacific Rise (EPR). Thus, the nature of the hydrothermal particles collected in the south Tonga arc is probably not drastically different from particles in the EPR region. However, we observed consistent differences between the two sites within the Tonga arc, in terms of the contribution of non-biogenic material, the radiocarbon content of sinking particulate organic carbon, the ratios of iron to other metals (e.g. Cu/Fe and Zn/Fe), and plume maturity indices (e.g. S/Fe). This heterogeneity within the Tonga arc is likely caused by differences in physical environment such as water depth, phase separation due to subcritical boiling and associated sub-seafloor precipitation.

1. Introduction

Submarine hydrothermal systems are found along mid ocean ridges (~ 60,000 km) and volcanic arcs (~23,000 km), including the spreading centers of back arc basins (de Ronde et al., 2001; Baker et al., 2006; Hawkes et al., 2014). An estimated 9% of global hydrothermal water flux flows through the hydrothermal systems of volcanic arcs (Baker et al., 2008).

Differences in the physical environments of hydrothermal systems (e.g. arc volcanoes versus mid ocean ridges) result in differences in the characteristics of their hydrothermal plumes and underlying deposits (Gamo et al., 2004; Hannington et al., 2005; Butterfield et al., 2011; de Ronde et al., 2001, 2011; Leybourne et al., 2012). Furthermore, the geochemical properties of a hydrothermal plume and the authigenic particles emanating from it depend on various factors, such as host-rock composition, water depth, and phase separation by subcritical boiling (de Ronde et al., 2001; Baker et al., 2006; Stoffers et al., 2006; Hawkes et al., 2013).

Existing studies of volcanic arcs focus mainly on hydrothermal plumes and their underlying deposits (Hannington et al., 2005; Massoth et al., 2007; Resing et al., 2007). Studies of sinking particles emanating from arc volcanoes may allow us to better understand mass transformation processes between hydrothermal plumes and deposits. Yet, the characteristics of sinking particles associated with these hydrothermal vent fields have not been studied due to sampling difficulties.

* Corresponding author.
E-mail addresses: juac29@kiost.ac.kr (H.J. Kim), jukim@kiost.ac.kr (J. Kim), electrum@kiost.ac.kr (S.J. Pak), sjju@kiost.ac.kr (S.-J. Ju), cmyoo@kiost.ac.kr (C.M. Yoo), hyskim@kiost.ac.kr (H.S. Kim), kylee@kiost.ac.kr (K.Y. Lee), jeomshik@snu.ac.kr (J. Hwang).

http://dx.doi.org/10.1016/j.dsr.2016.07.015
0967-0637/

We report the biogeochemical properties of sinking particles associated with the hydrothermal systems of a volcanic arc. We examined sinking particles collected by short term deployments of sediment traps around hydrothermal vent fields in the south Tonga arc. We compared the fluxes and compositions of sinking particles at two hydrothermal sites situated close to one another, but at different water depths and of different venting types. We also compare our results with previous studies of sinking particles associated with hydrothermal environments in divergent boundaries (such as the EPR, East Pacific Rise). Our study provides an opportunity to explore the similarity and difference in sinking particle flux and composition among various types of hydrothermal systems.

2. Methods

2.1. Study area

The Tonga arc lies between the southern end of the Eastern Lau Spreading Center and the intraoceanic arc front in the western Pacific (de Ronde et al., 2003). Submarine volcanoes and hydrothermal vents have been found at various water depths along the Tonga arc (Herzig et al., 1993, 1998; de Ronde et al., 2003; Stoffers et al., 2006). Many low-temperature steam vents have been observed at the summits and feet of shallow submarine volcanoes, while high-temperature black smoker vents have been found only in the deepest calderas, at water depths in excess of 1 km (de Ronde et al., 2001; Stoffers et al., 2006).

KIOST (Korea Institute of Ocean Science and Technology, formerly known as KORDI) surveyed two volcanoes with abundant mineral deposits (namely Volcano 18S and Volcano 19 in Massoth et al. (2007)) in the south Tonga arc during a cruise in January-February 2012 (SMST 2012; Fig. 1). Volcano 19 has a large central cone complex in the east and a younger caldera, 1.9 km in diameter, in the west (Fig. 1) (Stoffers et al., 2006; Massoth et al., 2007). The summit of the cone of Volcano 19 was observed to be composed of three small calderas on which hydrothermal chimneys were found. Active chimneys were mostly located within the 50 m-diameter region on the summit. The fluid temperature was up to 240 °C (fluid temperatures were measured using a high temperature probe of the ROV). Active chimney structures were mostly medium temperature type with high Zn content or medium-to-low temperature type with relatively low Zn content. Fe-oxyhydroxides crust and Fe crust were found on the summit. Diffuse vents were observed outside this central region.

Volcano 18S has a large funnel-shaped caldera ~6.5 km in diameter and >1500 m in depth in the west and a cone in the east (Fig. 1) (Stoffers et al., 2006; Massoth et al., 2007). The western boundary of the caldera was at a water depth of ~900 m. Hydrothermal vents were observed in two regions at this site: on the western inner caldera wall and on the eastern caldera wall (Fig. 1). Most of the hydrothermal vents on the western wall of the caldera were actively venting high temperature fluid (up to 231 °C) and were relatively small (less than a few meters tall). Hydrothermal chimneys were found on the eastern side of the caldera at

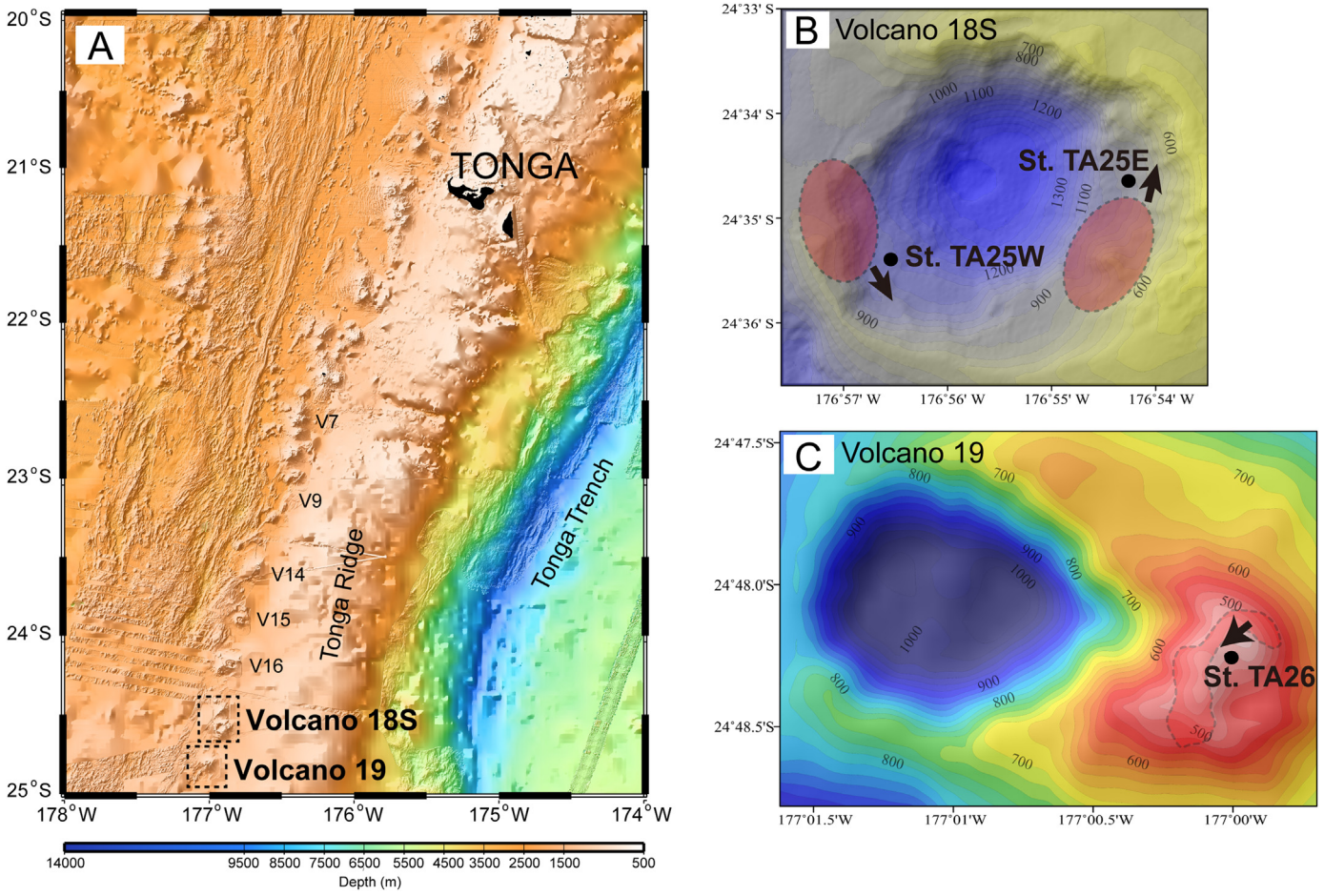

Fig. 1. Location of the study region (A) showing the stations at the two sites where the three traps were moored. Areas shaded in red in (B) and (C) indicate identified vent fields. Arrows around the trap-mooring sites denote the bottom current direction. (For interpretation of the references to color in this figure legend, the reader is referred to the web version of this article.)

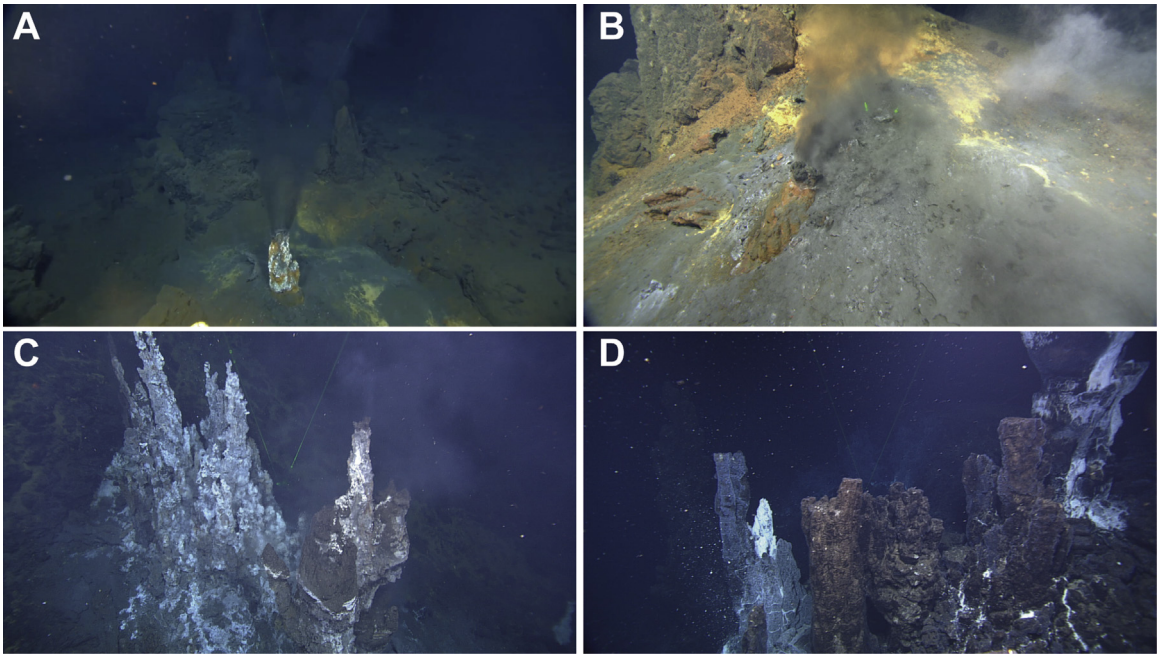

Fig. 2. Photos of vent sites. (A) and (B): Black smoker chimneys observed near TA25E; ~ 1 m tall; venting fluid temperature up to 263 °C. (C) and (D): Diffuse flow chimneys observed near TA26; fluid temperature up to 240 °C.

a water depth of about 930 m. The hydrothermal chimneys on the eastern caldera wall were different in size and type (e.g., chemical composition and venting type) from those on the western wall. In a 400 m by 80 m region, 34 hydrothermal structures including black smokers and other copper-containing chimneys and low temperature chimneys were observed on ROV survey. Most chimneys were taller than 10 m in height and were inactive although some chimneys were releasing low-temperature fluid. Low temperature type, inactive silica chimneys were also found. Noteworthy was the presence of three active black smoker chimneys (all 1–2 m high and with fluid temperatures up to 263 °C) (Fig. 2). Diffuse vents were found at the periphery of the central chimney region.

2.2. Sampling methods

Conical sediment traps (each 116 cm in height with a 0.25 m^2 opening) were deployed at the three sites described above (Fig. 1). Prior to deployment, the sampling cup of each sediment trap was filled with seawater treated with a sodium borate-buffered 10% formalin solution. Each sediment trap was gently placed on the seafloor by an ROV. To minimize the collection of unwanted sediment particles (resuspended due to disturbance caused by the ROV operation), each trap was deployed with the bottom of its collection funnel plugged, and the plug was subsequently removed by a robotic manipulator. No disturbance was detected visually when the traps were deployed.

Current speeds were measured using a moored Acoustic Doppler Current Profiler (ADCP). Sediment traps were deployed leeward of the bottom currents for efficient collection of sinking particles emanating from the vent fields.

One sediment trap was deployed on the eastern slope of Volcano 19, near the top of the cone, at a water depth of 460 m (Fig. 1). At this station (station TA26; 24°48.25′S, 177°00.02′W), sinking particles were collected for 11 days, from January 31, 2012 onward. Station TA26 lies within ~150 m of an identified hydrothermal vent; sediment trap deployment immediately adjacent to a vent was not possible because of the steeply sloped terrain. The fluid temperature at station TA26 was 160–240 °C. At station TA26, the direction of the current in the near-bottom layer was toward the southwest (Fig. 1C). Two sediment traps were deployed on Volcano 18S: one on the eastern caldera wall at a depth of 930 m (station TA25E; 24°34.68′S, 176°54.26′W) and one on the western caldera wall at a depth of 1150 m (station TA25W; 24°35.47′S, 176°56.55′W). Sinking particles were collected for 9 days (from February 7, 2012 on) at station TA25E, and for 16 days (from February 4, 2012 on) at station TA25W. Both stations were within ~200 m of identified vents. Bottom current directions at stations TA25W and TA25E were toward the southeast and northeast, respectively (Fig. 1B). When the trap at station TA25W was recovered, the ROV maneuver caused vigorous resuspension of sediment; sediment resuspension was not observed when the other two traps were recovered.

2.3. Analytical methods

Samples from the three sediment traps were stored in the dark at 4 °C, until analysis. Samples were rinsed three times with ultrapure (Milli-Q) water to remove residual formalin and then freeze-dried. Total mass flux was determined gravimetrically. Freeze-dried samples were analyzed for total carbon, using an elemental analyzer (Carlo-Erba 1110 CNS); for calcium carbonate ($CaCO_3$), using a carbon analyzer (UIC CO_2 coulometer, model CM5014); and for biogenic silica, using a time-series sequential dissolution method (DeMaster, 1981; Kim et al., 2011). For total carbon measurements, the analytical precision was better than 1.2% (1 relative standard deviation, RSD); better than 1% (1 RSD) for $CaCO_3$; and better than 3% (1 RSD) for biogenic silica. Organic carbon (OC) content was estimated as the difference between total carbon and total inorganic carbon. Non-biogenic material content was estimated as the difference between the total amount and biogenic material (two times OC + $CaCO_3$ + biogenic silica) (Fischer and Wefer, 1996; Palanques et al., 2002).

For metal analysis, about 100 mg of each sample was dissolved in a mixture of HF, HNO_3, and $HClO_4$ (HF:HNO_3:$HClO_4$=4:4:1) at 150 °C for 12 h. After evaporation, the residue was redissolved with 2% nitric acid (German et al., 1999, 2002). Concentrations of metals were determined using an ICP-AES (Al, Mg, Fe, S, Ba, Ti, Zn,

V, and P; Optima 4300 DV) and an ICP-MS (Mn, Cu, and Pb; X5 Thermo Elemental) at the Korea Basic Science Institute. A marine sediment standard (MESS-3, NRCC) was used as a certified reference material. The analytical recovery obtained from the analysis of the certified reference material ranged between 82% and 107% (Table 2). In particular, the analytical recovery of elemental sulfur and Fe was 90% and 99%, respectively. Relative standard deviations for metal analysis based on duplicate analysis of standard reference material were $\leq 10\%$. The reported concentrations are not corrected for analytical recovery.

For carbon isotope analysis, a fraction of dried sample was weighed in a silver cup and exposed to concentrated HCl vapor in a desiccator for ~12 h at room temperature to remove inorganic carbon (Hedges and Stern, 1984). The HCl-treated sample was packed in a quartz tube with CuO, evacuated on a vacuum manifold, flame-sealed, and combusted at 850 °C for 5 h. The resulting CO_2 gas was cryogenically purified. Carbon isotope ratios were measured at the National Ocean Sciences Accelerator Mass Spectrometry Facility at the Woods Hole Oceanographic Institution (McNichol et al., 1994).

3. Results

The daily-averaged current speed (100 m above the bottom) near station TA26 varied from 5.3 cm s^{-1} to 10.5 cm s^{-1} (7.4 cm s^{-1} on average). Near station TA25E, average current speed (100 m above the bottom) was 3.0 cm s^{-1} with a maximum speed of 3.8 cm s^{-1}. The observed current speed was not strong enough to influence the trapping efficiency or to cause considerable local sediment resuspension (Lampitt, 1985; Gust et al., 1992).

The total mass flux was 135 mg m^{-2} d^{-1} at TA26 and 105 mg m^{-2} d^{-1} at TA25E (Fig. 3a and Table 1). However, the total mass flux at TA25W was distinctly higher (854 mg m^{-2} d^{-1}) than at the two other sites, suggesting that this sample was compromised by the inclusion of sediment particles resuspended by the ROV maneuver during recovery. Hence, we considered the concentration data from this sample as representative of the surface sediment, and only used these data for the comparison between authigenic sinking particles and surface sediments.

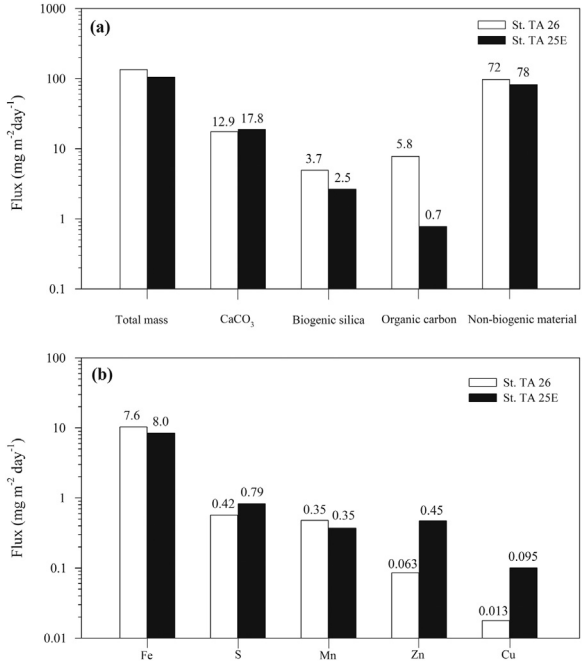

Fig. 3. Fluxes at the two sites of (a) sinking materials and (b) elements. Note that the y-axes are on a logarithmic scale. The values above the bars are concentrations in per cent.

Biogenic material accounted for 28% of sinking particle at TA26 and 22% of sinking particle at TA25E (Table 1). $CaCO_3$ accounted for a higher fraction of biogenic particles than biogenic silica (Table 1). Although most biogenic components were present at comparable levels at Volcano 19 and Volcano 18 S, organic carbon content differed considerably (Table 1). Radiocarbon content ($\Delta^{14}C$) of particulate organic carbon was −189‰ at TA26 and −462‰ at TA25E. Stable isotope measurements yielded a $\delta^{13}C$ value of −23.0‰ at TA26 and −24.3‰ at TA25E. In comparison, the $\Delta^{14}C$ and $\delta^{13}C$ values at TA25W were −76‰ and −21.4‰, respectively.

Non-biogenic material accounted for the largest fraction (over 70% at each station) of sinking particles (Table 1). Non-biogenic material was dominated by Fe (about 8.0% of sinking particles), followed by Al (4–5%), and Mg (1–2%) (Table 1). Mn, S, and Ti contents ranged between 0.2% and 0.8% and were present at levels similar to or higher than Cu, Zn, Cr, and Sr (Table 2). Fe fluxes at TA26 and TA25E were 10 and 8 mg m^{-2} d^{-1}, respectively (Fig. 3b and Table 1). Sulfur fluxes were 0.6 and 0.8 mg m^{-2} d^{-1}, which accounted for 0.4% and 0.8% of sinking particles at TA26 and TA25E, respectively (Fig. 3b and Table 1). Mn fluxes were 0.5 and 0.4 mg m^{-2} d^{-1} at TA26 and TA25E, respectively, accounting for about 0.4% of sinking particles at each station (Fig. 3b and Table 1). Concentrations of Cu, Zn, and Cr were several-fold higher at TA25E than at TA26. Concentrations of most other metals were comparable at the two sites.

The ground particle samples were examined by X-ray diffraction (XRD). The XRD patterns qualitatively showed that sulfur containing minerals (sphalerite, pyrite, and marcasite) were more abundant at TA25E than at TA26. Quartz and anorthite were more abundant than sulfide minerals at TA26.

4. Discussion

4.1. Biogenic vs. authigenic sources of sinking particles

The total mass flux we observed is several-fold higher than fluxes (11–32 mg m^{-2} d^{-1}) reported for non-hydrothermal sites in the southwest subtropical Pacific (Honjo et al., 2000; Nodder and Northcote, 2001; Kawahata, 2002). This high particle flux, the high contribution of non-biogenic material (over 70%) and the considerably elevated flux of metals such as Fe, Mn, Cu, and Zn, indicate that hydrothermal authigenic particles were an overwhelmingly dominant source of the collected particles (Fig. 3). Although the observed total mass fluxes (135 and 105 mg m^{-2} d^{-1} at TA26 and TA25E, respectively) were one to two order(s) of magnitude lower than those (0.8–11.6 g m^{-2} d^{-1}) observed immediately adjacent to vents in other vent fields, our particle flux results are in keeping with trends previously observed between total mass flux and distance from a vent (not shown; Fig. 2 of German et al., 2002).

The Al/(Al + Mn + Fe) ratios that we observed (0.31 and 0.36 at TA26 and TA25E, respectively), were significantly lower than for lithogenic material (> 0.5) (Bostrom and Peterson, 1969; Mills and Elderfield, 1995; German et al., 2002). The value of this ratio at TA25W (0.43) suggests that the non-biogenic component of the underlying non-biogenic surface sediment is also mostly derived from authigenic particles. On a plot of Al/(Al + Fe + Mn) versus Fe/Ti (Fig. 4), the values at both stations (TA26 and TA25E) are positioned between continental crust values and values for hydrothermal particles collected immediately adjacent to a vent at the Endeavour segment (Bostrom and Peterson, 1969; Peter and Goodfellow, 1996; Hrischeva and Scott, 2007). Note however, that contribution of hydrothermal Al at volcanic arc settings such as

Table 1
Particle flux and relative contributions of biogenic and non-biogenic materials to sinking particles at three sites in the Tonga arc.

	Fluxes in mg m^{-2} d^{-1} (% of total mass flux)									
	Total mass	$CaCO_3$	Biogenic silica	Organic carbon	Non-biogenic material	Al	Fe	Mn	S	Ti
TA26	135	17.5 (12.9)	4.9 (3.7)	7.8 (5.8)	97 (72)	4.7 (3.6)	10.3 (7.6)	0.5 (0.35)	0.6 (0.42)	0.3 (0.22)
TA25E	105	18.8 (17.8)	2.6 (2.5)	0.78 (0.7)	82 (78)	5.0 (4.7)	8.4 (8.0)	0.4 (0.35)	0.8 (0.79)	0.3 (0.28)
TA25W	854	117 (13.4)	28.8 (3.4)	9.5 (1.1)	690 (81)	51 (6.0)	63 (7.4)	5.0 (0.59)	26.5 (3.1)	2.5 (0.29)
Non-hydrothermal Southwestern Pacific[a]	11 – 32	7 – 20 (62 – 77)	0.5 – 1.2 (5 – 7)	1.0 – 2.3 (5 – 9)	1.1 – 3.4 (8 – 13)	–	–	–	–	–

[a] Data from Nodder and Northcote (2001) and Kawahata (2002).

Table 2
Elemental concentrations of sinking particles. Excess values for each element are estimated from the measured concentration and then normalized to Ti (see text). Upper continental crust values are presented for comparison. Analytical recovery for each element based on the analysis of a standard reference material is also presented.

		Al (%)	Mg (%)	Fe (%)	Mn (%)	S (%)	Ba (%)	Ti (%)	Cu (ppm)	Zn (ppm)	Pb (ppm)	V (ppm)	P (ppm)
TA26	Observed	3.6	2.0	7.6	0.35	0.42	0.63	0.22	1.3E+2	6.3E+2	8.0E+2	2.1E+2	2.2E+4
	EE (% of measured)	0.64 (18%)	–	6.5 (85%)	0.33 (94%)	–	0.61 (96%)	–	1.2E+2 (92%)	6.0E+2 (96%)	8.0E+2 (99%)	1.7E+2 (81%)	–
TA25E	Observed	4.7	1.4	8.0	0.35	0.79	2.16	0.28	9.5E+2	4.5E+3	4.8E+2	1.7E+2	1.9E+3
	EE (% of measured)	0.93 (20%)	–	6.6 (82%)	0.32 (91%)	–	2.14 (99%)	–	9.4E+2 (99%)	4.5E+3 (99%)	4.7E+2 (98%)	1.2E+2 (71%)	–
TA25W	Observed	6.0	2.1	7.4	0.59	3.1	0.63	0.29	1.3E+2	2.7E+2	1.2E+2	2.8E+2	2.3E+2
	EE (% of measured)	2.1 (35%)	–	5.9 (80%)	0.56 (95%)	–	0.61 (96%)	–	1.1E+2 (89%)	2.3E+2 (86%)	1.1E+2 (92%)	2.2E+2 (82%)	–
Endeavour (2100 m)[a]	Observed	1.28	–	8.9	0.14		0.79	0.07	5.9E+3	1.8E+4	–	–	–
	EE (% of measured)	0.11 (8.3%)		8.4 (94%)	0.13 (94%)		0.78 (99%)		5.9E+3 (99%)	1.8E+4 (99%)			
Continental crust[b]		8.04	1.35	3.50	0.06	–	0.05	0.6	25	71	17	107	665
MESS-3[c]	Certified value	8.59	1.6	4.34	0.32	0.19	–	0.44	33.9	159	21.1	243	1200
	Measured value	7.84	1.7	4.29	0.32	0.17	–	0.42	31.3	133	19.0	209	988
	Recovery (%)	91	107	99	99	90	–	96	93	83	89	86	82

[a] Element data in hydrothermal particle at the Endeavour segment from Dymond and Roth (1988).
[b] Element data in the upper continental crust from Taylor and McLennan (1985) and Wedepohl (1995).
[c] Certified reference marine sediment (MESS-3, NRCC) analysis.

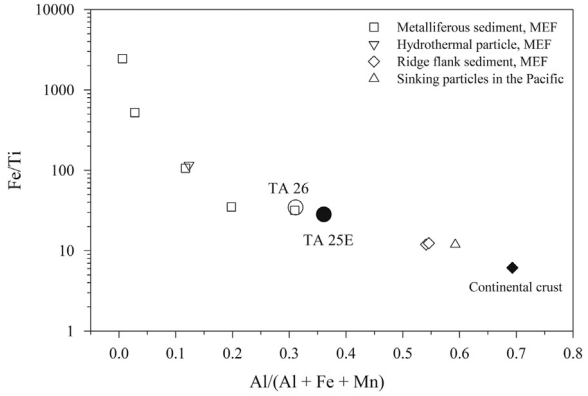

Fig. 4. Plot of Fe/Ti versus Al/(Al+Fe+Mn) showing variations in the relative amounts of hydrothermal and detrital components. Also shown are data from the Main Endeavour Field (MEF) in the Juan de Fuca ridge (Bostrom and Peterson, 1969; Dymond and Roth, 1988; Goodfellow and Peter, 1994); sinking particles in the Pacific (Dymond and Roth, 1988); and the average value of the continental crust (Taylor and McLennan, 1985). Note that the y-axis is on a logarithmic scale.

our sites is higher than at mid ocean ridge sites (see discussion later), and caution should be taken when this ratio is compared between different hydrothermal settings.

Because hydrothermal precipitates contribute little Ti (Feely et al., 1994; Cowen et al., 2001), the excess of each element (EE) over its average value in the upper continental crust (e.g., Ziegler et al., 2007) can be estimated using the Ti concentration in a sample and the ratio of Ti to each element in the upper continental crust, as follows:

$$EE = element_{meas} - \left[(element/Ti)_{crust} \times Ti_{meas} \right],$$

where $element_{meas}$ and Ti_{meas} denote the concentration of each element and Ti in a given sample, respectively, and $(element/Ti)_{crust}$ denotes the average ratio of an element in the upper continental crust (Taylor and McLennan, 1985). The percent contribution of EE to the corresponding element concentration in the sinking particle sample was $>80\%$ for Fe and $>90\%$ for Mn, Ba, Cu, Pb and Zn at both sites (Table 2). At TA25E, this value was especially high (99%) for Ba, Cu, and Zn. Our results are consistent with the percent contribution of EE observed in hydrothermal particles obtained from the Endeavour vent fields (Table 2) (Dymond and Roth, 1988), except for Al and Fe (see Section 4).

One reason for the slight difference in biogenic material content between the two sites (Table 1) may be the sampling depth: the shallower station, TA26, probably receives more biogenic material from the overlying euphotic zone than the deeper station, TA25E (Fig. 5). The $\Delta^{14}C$ values of sinking POC at both sites were distinctly lower than the value expected for freshly produced particulate organic matter in the overlying euphotic zone ($\sim +50‰$, Key et al., 2004). The $\Delta^{14}C$ value of dissolved inorganic carbon in a hydrothermal effluent reflects the relative strengths of

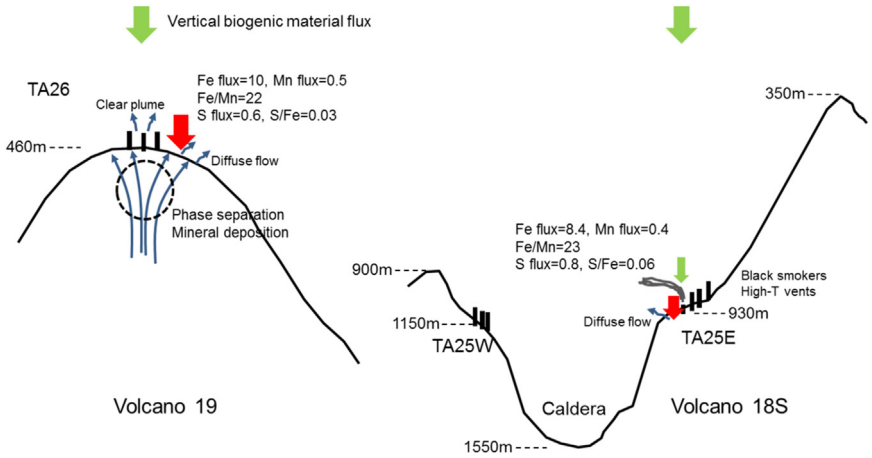

Fig. 5. A cartoon of the two volcanoes with the relative location of the study sites (note that the drawing is not in scale). The ratios between elements are all molar ratios. Flux values are presented in mg m^{-2} d^{-1}.

Table 3
Comparison of properties between TA26 and TA25E.

Properties	TA26 (Volcano 19)		TA25E (Volcano 18S)
Depth (m)	460	<	930
Vent type	Clear plume + diffuse vent		Black smoker + clear plume + diffuse vent
Temperature (°C)	160–240	<	263
Distance from vent (m)	~150	≤	~200
Non-biogenic material (%)	72	<	78
Phase separation (boiling)	Likely		No
% of excess Fe, Mn	85%, 94%	>	82%, 91%
% of excess Cu, Zn	92–96%	<	99%
Fe/Mn molar ratio	22	=	23
S/Fe molar ratio (maturity index)	0.03 (more mature)	<	0.06
Cu/Fe, Zn/Fe molar ratio (venting temperature index)	0.002, 0.01	<	0.017, 0.08
POC %	6	>	0.7
Biomass relying on ^{14}C-free carbon (based on Δ^{14}C and δ^{13}C)	−189‰ −23.0‰	<	−462‰ −24.3‰

its two sources: dissolved inorganic carbon in bottom seawater and ^{14}C-free ($\Delta^{14}C = -1000$‰) basaltic CO_2 (Proskurowski et al., 2004; Walker et al., 2008). In the same manner, the Δ^{14}C values of sinking POC reflect the mixing between chemosynthetically produced organic matter from the dissolved inorganic carbon in the vent fields and POC supplied from the overlying euphotic zone. However, it is not feasible to quantify the contribution of each POC source based on Δ^{14}C values of POC alone, without Δ^{14}C values for the hydrothermal plumes at our sites. Also, it is not known what fraction of chemoautotrophy utilizes inorganic carbon in the ambient seawater rather than ^{14}C-free carbon. Qualitatively, the lower Δ^{14}C value at TA25E than at TA26 (Table 3) suggests that sinking POC at TA25E contains more chemosynthetically produced organic matter than sinking POC at TA26 (where the water depth was shallower).

4.2. Variation of sinking particle properties within the south Tonga arc

Stoffers et al. (2006) reported that most plume temperatures (240–265 °C) of Volcano 19 were on the boiling curve. They reported vigorous two-phase venting, which was also observed by our ROV survey. Subcritical boiling influences the geochemical characteristics of hydrothermal plume and particles (Stoffers et al., 2006; Massoth et al., 2007). The difference of particle characteristics between TA25E and TA26 may be interpreted in this context.

Although higher sulfur flux was expected at TA25E considering the existence of black smokers, the observed sulfur flux was only slightly higher at TA25E than at TA26 (0.8 vs. 0.6 mg m^{-2} d^{-1}). Immediate precipitation of sulfur upon effusion of the fluid is likely a reason for this observation. Elemental sulfur, which may have been deposited from disproportionation reaction of SO_2 (Butterfield et al., 2011), was also observed near the black smokers and porous rocks at TA25E (Fig. 2B). The S/Fe molar ratio in hydrothermal particles has been used as an index to assess the maturation of a hydrothermal plume after effusion (e.g., Feely et al., 1994; Lilley et al., 1995; Hawkes et al., 2013). The S/Fe molar ratio immediately following an effusion (> 10) reportedly decreased (to 0.04-0.8) with time (Haymon et al., 1993; Lupton et al., 1993; Feely et al., 1994; Massoth et al., 1994; Lilley et al., 1995). The observed S/Fe molar ratios are consistent with precipitation from a mature effluent.

The observed S/Fe molar ratio at TA26 (0.03) was towards the lower end of the observed values. The low particulate sulfur flux at TA26 was likely caused by precipitation below seafloor before effusion of the plume. The difference in the ratio of S/Fe, Cu/Fe, and Zn/Fe between the two sites may be consistently explained by this mechanism. Stoffers et al. (2006) suggested that boiling beneath Volcano 19 may possibly extend well below the volcano's summit, which could cause sub-seafloor deposition of chalcophiles. Effusion of clear plume, which is depleted with volatile gases, and diffuse plume at TA26 also supports that initial precipitation occurs before plume effusion. Sulfur and chalcophile elements such as Zn and Cu are expected to precipitate underneath the seafloor.

The observed low S/Fe ratios imply that particulate Fe was likely in the form of oxyhydroxide rather than sulfide. This conjecture is consistent with the observation of rusty Fe-oxyhydroxide sediments around Volcano 19 (Stoffers et al., 2006). The XRD patterns consistently showed that aluminosilicate minerals (Quartz and anorthite) were more abundant than sulfide minerals at TA26. Bennett et al. (2011) used V to Fe ratio to apportion hydrothermal Fe particles into Fe-oxyhydroxide and Fe-sulfide. When we adopted this approach using 0.0046 as the ratio of V/Fe for the Kemp caldera of volcanic arc setting (Hawkes et al., 2014), an inconsistently high portion (~50%) was estimated to be in Fe-sulfide. The V/Fe ratio in oxyhydroxide varies depending on phosphate concentrations (Feely et al., 1998) and possibly on other parameters. Therefore, care should be taken when this approach is

adopted. For example, a much lower value of 0.0026 was observed at Rota-1 of the Mariana volcanic arc (Resing et al., 2007).

Data of metal concentrations in the hydrothermal plume in the study region for comparison with our sinking particle data are rare and were obtained in 2003 (Massoth et al., 2007). The ratios of total dissolvable Fe to Mn in the plume were 1.2 ± 0.3 and 1.8 ± 0.4 at the caldera of Volcano 18 S and at the summit of Volcano 19, respectively (Massoth et al., 2007). The fluxes of sinking particulate Mn and Fe were comparable at both sites (0.5 and 0.4 mg m^{-2} d^{-1} for Mn and 10.4 and 8.4 mg m^{-2} d^{-1} for Fe at TA26 and TA25E, respectively). As a result, the Fe/Mn ratio in sinking particles was similar at both sites (22–23; Table 3). The Fe/Mn ratios in sinking particles were one order of magnitude higher than that of the plume observed in 2003. However, care should be taken for this comparison because of possible temporal variation in the plume characteristics. Fe precipitates from the plume to particles preferentially than Mn by becoming incorporated into metal sulfides and Fe-oxyhydroxides that settle down faster and closer to the chimney (Marchig and Gundlach, 1982; Mottl and McConachy, 1990; German et al., 1999). Although Mn may also co-precipitate with Fe-oxyhydroxide (Hawkes et al., 2014), particulate Mn may stay suspended as fine particles before incorporated into sinking (large-sized) particles. Massoth et al. (2007) reported enrichment of Mn inside the caldera of the volcanoes as reflection of aging of the plumes.

4.3. Comparison with other hydrothermal environments

Flux and elemental composition of sinking particles from a hydrothermal plume may change rapidly with time upon effusion from the vent. Because our results are limited to a single point from each vent field, the distance between the vents and sample collection sites is a key variable to consider when they are compared with the literature data. We compared our results with studies of other major hydrothermal vent fields, by examining indices such as the ratios of metal elements that are indicative of the geochemical properties of hydrothermal plumes. The Fe/Mn ratio in authigenic particles varies with their distance from the vent (Marchig and Gundlach, 1982; Mottl and McConachy, 1990; German et al., 1999). For example, the Fe/Mn molar ratio in the hydrothermal particles at the Totem vent field of the EPR decreased from 358 at a 5 m distance from the chimney, to 194 at 20 m, and 9 at 300 m from the chimney (German et al., 2002). The Fe/Mn molar ratios (22–23) we observed and the distance of our sites from vents (150–200 m) appear to fit the trend observed at the Totem vent in the EPR (German et al., 2002).

The observed S/Fe molar ratio (0.06) at TA25E is consistent with precipitation from a mature effluent (Table 3). Similarly, the molar ratios of chalcophiles to iron (Cu/Fe and Zn/Fe) in sinking particles at TA25E compare well with the results from the Totem vent fields (Cu/Fe: 0.008–0.018, Zn/Fe: 0.027–0.37), buoyant plume particles from immediately above the 21°N EPR site (Cu/Fe: 0.02–0.03, Zn/Fe: 0.32–0.36), and neutrally buoyant plume material (Cu/Fe: 0.025, Zn/Fe: 0.018) taken from between 9° and 10°N in the EPR (Fig. 6) (Mottl and McConachy, 1990; Khripounoff and Alberic, 1991; Feely et al., 1994; German et al., 2002). However, on a plot of Cu/Fe versus Zn/Fe, data from TA26 do not fit the general trend line observed at divergent boundary sites (Fig. 6). Low S/Fe, Cu/Fe, and Zn/Fe ratios at TA26 may have been caused by subcritical boiling and sub-seafloor precipitation as discussed earlier.

A difference between our sites and other hydrothermal systems was found in the contribution of Al. The percent contribution of Al excess at our sites was 18–20% (Table 2), whereas the hydrothermal discharge from vents at mid ocean ridges was smaller (Dymond and Roth, 1988; Feely et al., 1994; Gamo et al., 1997). For example, the percent contribution of Al excess to total Al

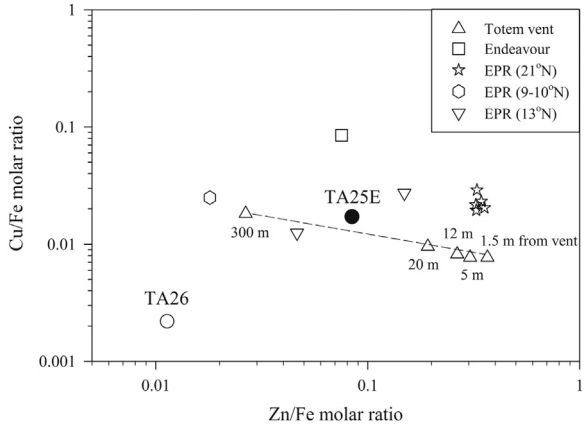

Fig. 6. A plot of the Cu/Fe molar ratio versus the Zn/Fe molar ratio from our study. Also shown, for comparison, are the data of hydrothermal particle and buoyant plume particles for the Endeavour segment, Totem vent, and EPR (9–21°N) from Dymond and Roth (1988), Mottl and McConachy (1990), Khripounoff and Alberic (1991), Feely et al. (1994), and German et al. (2002).

concentration was only 8.3% at the Endeavour vent fields in the Juan de Fuca ridge (Table 2) (Dymond and Roth, 1988). Al leaches from silicate minerals under the highly acidic conditions caused by the input of magma-derived SO_2 at convergent margins (Stoffregen, 1987; Gamo et al., 1997, 2004; Resing et al., 2007; Butterfield et al., 2011). Resing et al. (2007) reported that particulate Al concentration was over 1000 nM in the plume of NW Rota-1 on the Mariana arc. This kind of high Al concentration has not been observed in plumes of other hydrothermal settings. The relatively high contribution of Al excess in our study region may be characteristic of hydrothermal fluids emanating from arc volcanoes.

5. Summary and conclusions

Our study provides initial results of the flux and elemental composition of the sinking particles in the south Tonga volcanic arc of the convergence boundary. The characteristics of sinking particles emanating from hydrothermal vent fields in the convergent plate boundary were insufficient to compare the geochemical properties of hydrothermal systems in the mid ocean ridge region due to limitation of data.

We deployed sediment traps over the short term (~10 days) at two sites, each 150–200 m away from identified hydrothermal vents. The total mass flux was several-fold higher than in the non-hydrothermal southwest tropical Pacific. The contribution of non-biogenic materials was dominant (over 72% of total sinking particles). Metals such as Fe, Mn, Cu, and Zn were present in great excess compared to their average levels in the upper continental crust, indicating that hydrothermal authigenic particles were the dominant source of the collected sinking particles.

Comparisons of sinking particles collected at the two sites (which were at different water depths) suggest that the hydrothermal plumes and particle precipitation of the Tonga volcanic arc have heterogeneous characteristics. Phase separation at TA26 due to subcritical boiling and sub-seafloor precipitation of particles appears to be reflected by the relatively low values of S/Fe, Cu/Fe, and Zn/Fe ratios.

Within the limitation of our data at single point, 150–200 m off the source, the indices developed from data gathered at sites along divergent plate boundaries appear to be valid for our sites, although ours were located along a convergent boundary volcanic arc. The total particle fluxes that we observed varied with distance from the source vent in a manner similar to trends observed at

divergent boundaries. In addition, both the relationship between Fe/Ti and Al/(Al+Fe+Mn), and the relationship between Cu/Fe and Zn/Fe, also appear to be in synchrony with results from divergent plate sites. However, heterogeneity in particle characteristics within the Tonga volcanic arc complicates the comparison between our study sites and data from other hydrothermal environments. Nonetheless, our observations suggest that the nature of hydrothermal particles at the south of Tonga arc is not drastically different from particles collected in the EPR region, with the potential exception that subcritical boiling may imbue authigenic particles with distinct characteristics.

Acknowledgements

We thank Eung Kim and Dong Guk Kim for help with the operation of the sediment trap and the captain and crew of the R/V SONNE for their assistance during the survey cruise. This research was supported by the Korean Government's Ministry of Ocean and Fisheries (PM57063 and PM58902) and a KIOST internal research (PE99397).

References

Baker, E., Resing, J., Walker, S., Martinez, F., Taloy, B., Nakamura, K., 2006. Abundant hydrothermal venting along melt-rich and melt-free ridge segments in the Lau back-arc basin. Geophys. Res. Lett. 33, L07308. http://dx.doi.org/10.1029/2005GL025283.

Baker, E., Embley, R., Walker, S., Resing, J., Lupton, J., Nakamura, K., de Ronde, C., Massoth, G., 2008. Hydrothermal activity and volcano distribution along the Mariana arc. J. Geophys. Res. 113, B08S09. http://dx.doi.org/10.1029/2007JB005423.

Bennett, S.A., Statham, P.J., Green, D.R.H., Bris, N.L., McDermott, J.M., Prado, F., Rouxel, O.J., von Damm, K., German, C.R., 2011. Dissolved and particulate organic carbon in hydrothermal plumes from the East Pacific Rise, 9°50′N. Deep-Sea Res. I 58, 922–931.

Bostrom, K., Peterson, M.M.A., 1969. The origin of aluminum-poor ferromanganoan sediments in areas of high heat flow on the East Pacific Rise. Mar. Geol. 7, 427–447.

Butterfield, D.A., Nakamura, K., Takano, B., Lilley, M., Lupton, J., Resing, J., Roe, K., 2011. High SO_2 flux, sulfur accumulation, and gas fractionation at an erupting submarine volcano. Geology 39, 803–806.

Cowen, J.P., Betram, M.A., Wakeham, S.G., Thomson, R.E., Lavelle, J.W., Baker, E.T., Feely, R.A., 2001. Ascending and descending particle flux from hydrothermal plumes at Endeavour Segment, Juan de Fuca Ridge. Deep-Sea Res. I 48, 1093–1120.

DeMaster, D.J., 1981. The supply and accumulation of silica in the marine environment. Geochim. Cosmochim. Acta 45, 1715–1732.

de Ronde, C., Baker, E., Massoth, G., Lupton, J., Wright, I., Feely, R., Greene, R., 2001. Intra-oceanic subduction-related hydrothermal venting, Kermadec volcanic arc, New Zealand. Earth Planet. Sci. Lett. 193, 359–369.

de Ronde, C., Faure, K., Bray, C.M., Chappell, D., Wright, I., 2003. Hydrothermal fluids associated with seafloor mineralization at two southern Kermadec arc volcanoes, offshore New Zealand. Miner. Depos. 38, 217–233.

de Ronde, C., Massoth, G., Butterfield, D., Christenson, B., Ishibashi, J., Ditchburn, R., Hannington, M., Brathwaite, R., Lupton, J., Kamenetsky, V., Graham, I., Zellmer, G., Dziak, R., Embley, R., Dekov, V., Munnuk, F., Lahr, J., Evans, L., Takai, K., 2011. Submarine hydrothermal activity and gold-rich mineralization at Brothers Volcano, Kermadec Arc, New Zealand. Miner. Depos. 46, 541–584.

Dymond, J., Roth, S., 1988. Plume dispersed hydrothermal particles: a time-series record of settling flux from the Endeavour Ridge using moored sensors. Geochim. Cosmochim. Acta 52, 2525–2536.

Feely, R.A., Gendron, J.F., Baker, E.T., Lebon, G.T., 1994. Hydrothermal plumes along the East Pacific Rise, 8°40′ to 11°50′N: particle distribution and composition. Earth Planet. Sci. Lett. 128, 19–36.

Feely, R.A., Trefry, J.H., Lebon, G.T., German, C.R., 1998. The relationship between P/Fe and V/Fe ratios in hydrothermal precipitates and dissolved phosphate in seawater. Geophys. Res. Lett. 25, 2253–2256.

Fischer, G., Wefer, G., 1996. Seasonal and interannual particle fluxes in the Eastern Equatorial Atlantic from 1989 to 1991: ITCZ migration and upwelling. In: Ittekkot, V., Schafer, P., Honjo, S., Depetris, P.J. (Eds.), Particle Flux in the Ocean (SCOPE). John Wiley & Sons Ltd, New York, pp. 199–214.

Gamo, T., Okamura, K., Charlou, J.L., Urabe, T., Auzende, J.M., Shipboard Scientific Party of the ManusFlux Cruise, Ishibashi, J., Shitashima, K., Kodama, Y., 1997. Acidic and sulfate-rich hydrothermal fluid from the Manus basin, Papua New Guinea. Geology 25, 139–142.

Gamo, T., Masuda, H., Yamanaka, T., Okamura, K., Ishibashi, J., Nakayama, E., Obata, H., Shitashima, K., Nishio, Y., Hasumoto, H., Watanabe, M., Mitsuzawa, K., Seama, N., Tsunogai, U., Kouzuma, F., Sano, Y., 2004. Discovery of a new hydrothermal venting site in the southernmost Mariana Arc: Al-rich hydrothermal plumes and white smoker activity associated with biogenic methane. Geochem. J. 38, 527–534.

German, C.R., Hergt, J., Palmer, M.R., Edmond, J.M., 1999. Geochemistry of a hydrothermal sediment core from the OBS vent-field, 21°N East Pacific Rise. Chem. Geol. 155, 65–75.

German, C.R., Colley, S., Palmer, M.R., Khripounoff, A., Klinkhammer, G.P., 2002. Hydrothermal plume-particle fluxes at 13°N on the East Pacific Rise. Deep-Sea Res. I 49, 1921–1940.

Goodfellow, W.D., Peter, J.M., 1994. Geochemistry of hydrothermally altered sediment, Middle Valley, northern Juan de Fuca Ridge. In: Davis, E.E., Mottl, M.J., Fisher, A.T. et al. (eds). Proceedings of the Ocean Drilling Program (ODP), College Station, TX, Scientific Results, vol. 139, pp. 207–289.

Gust, G., Byrne, R.H., Bernstein, R.E., Betzer, P.R., Bowles, W., 1992. Particle fluxes and moving fluids: experience from synchronous trap collections in the Sargasso Sea. Deep-Sea Res. 39, 1071–1083.

Hannington, M., de Ronde, C., Petersen, A., 2005. Sea-floor tectonics and submarine hydrothermal systems. Econ. Geol. 100, 111–141.

Hawkes, J.A., Connelly, D.P., Gledhill, M., Achterberg, E.P., 2013. The stabilisation and transportation of dissolved iron from high temperature hydrothermal vent systems. Earth Planet. Sci. Lett. 375, 280–290.

Hawkes, J.A., Connelly, D.P., Rijkenberg, M.J.A., Achterberg, E.P., 2014. The importance of shallow hydrothermal island arc systems in ocean biogeochemistry. Geophys. Res. Lett. http://dx.doi.org/10.1002/2013GL058817

Haymon, R.M., Fornari, D.J., von Damm, K.L., Lilley, M.D., Perfit, M.R., Edmond, J.M., Shanks, W.C., Lutz, R.A., Grebmeier, J.M., Carbotte, S., Wright, D., McLaughlin, E., Smith, M., Beedle, N., Olson, E., 1993. Volcanic eruption of the mid-ocean ridge along the East Pacific Rise crest at 9°45-52′N: Direct submersible observations of seafloor phenomena associated with an eruption event in April 1991. Earth Planet. Sci. Lett. 119, 85–101.

Hedges, J.I., Stern, J.H., 1984. Carbon and nitrogen determinations of carbonate-containing solids. Limnol. Oceanogr. 29, 657–663.

Herzig, P.M., Hannington, M.D., Fouquet, Y., Stackelberg, U., Peterson, S., 1993. Gold-rich polymetallic sulfides from the Lau back arc and implications for the geochemistry of gold in sea-floor hydrothermal systems of the Southwest Pacific. Econ. Geol. 88, 2182–2209.

Herzig, P.M., Hannington, M.D., Arribas Jr., A., 1998. Sulfur isotopic composition of hydrothermal precipitates from the Lau back-arc: implications for magmatic contributions to seafloor hydrothermal systems. Miner. Depos. 33, 226–237.

Honjo, S., Francois, R., Manganini, S., Dymond, J., Collier, R., 2000. Particle fluxes to the interior of the Southern Ocean in the Western Pacific sector along 170°W. Deep-Sea Res. II 47, 352–3548.

Hrischeva, E., Scott, S.D., 2007. Geochemistry and morphology of metalliferous sediments and oxyhydroxides from the Endeavour segment, Juan de Fuca Ridge. Geochim. Cosmochim. Acta 71, 3476–3497.

Kawahata, H., 2002. Suspended and settling particles in the Pacific. Deep-Sea Res. II 49, 5647–5664.

Key, R.M., Kozyr, A., Sabine, C.L., Lee, K., Wanninkhof, R., Bullister, J.L., Feely, R.A., Millero, F.J., Mordy, C., Peng, T.H., 2004. A global ocean carbon climatology: results from Global Data Analysis Project (GDAP). Glob. Biogeochem. Cycles 18, GB4031. http://dx.doi.org/10.1029/2004GB002247.

Khripounoff, A., Alberic, P., 1991. Settling of particles in a hydrothermal vent field (East Pacific Rise 13ºN) measured with sediment traps. Deep-Sea Res. A 38, 729–744.

Kim, H.J., Kim, D., Yoo, C.M., Chi, S.B., Khim, B.K., Shin, H.R., Hyeong, K., 2011. Influence of ENSO variability on sinking-particle fluxes in the northeastern equatorial Pacific. Deep-Sea Res. I 58, 865–874.

Lampitt, R.S., 1985. Evidence for the seasonal deposition of detritus to the deep-sea floor and its subsequent resuspension. Deep-Sea Res. 32, 885–897.

Leybourne, M., Schwarz-Schampera, U., de Ronde, C., Baker, E., Faure, K., Walker, S., Butterfield, D., Resing, J., Lupton, J., Hannington, M., Massoth, G., Embley, R., Chadwick Jr, W., Clark, M., Timm, C., Graham, I., Wright, I., 2012. Submarine magmatic-hydrothermal systems at the Monowai volcanic centre, Kermadec Arc. Econ. Geol. 107, 1669–1694.

Lilley, M.D., Feely, R.A., Trefry, J.H., 1995. Chemical and biochemical transformations in hydrothermal plumes. Geophys. Monogr. Ser. 91, 369–391.

Lupton, J.E., Baker, E.T., Mottl, M.J., Sansone, F.J., Wheat, C.G., Resing, J.A., Massoth, G. J., Measures, C.J., Feely, R.A., 1993. Chemical and physical diversity of hydrothermal plumes along the East Pacific Rise, 8°45 to 11°50′N. Geophys. Res. Lett. 20, 2913–2916.

Marchig, V., Gundlach, H., 1982. Iron-rich metalliferous sediments on the East Pacific Rise: prototype of undifferentiated metalliferous sediments on divergent plate boundaries. Earth Planet. Sci. Lett. 58, 361–382.

Massoth, G.J., Baker, E.T., Lupton, J.E., Feely, R.A., Butterfield, D.A., von Damm, K.L., Roe, K.K., Lebon, G.T., 1994. Temporal and spatial variability of hydrothermal manganese and iron at Cleft segment, Juan de Fuca. J. Geophys. Res. 99, 4905–4923.

Massoth, G., Baker, E., Worthington, T., Lupton, J., de Ronde, C., Arculus, R., Walker, S., Nakamura, K.-I., Ishibashi, J.-I., Stoffers, P., Resing, J., Greene, R., Lebon, G., 2007. Multiple hydrothermal sources along the south Tonga arc and Valu Fa Ridge. Geochem. Geophys. Geosyst. 8, Q11008. http://dx.doi.org/10.1029/2007GC001675.

McNichol, A.P., Osborne, E.A., Gagnon, A.R., Fry, B., Jones, G.A., 1994. TIC, TOC, DIC, PIC, POC-unique aspects in the preparation of oceanographic samples for

^{14}C-AMS. Nucl. Instrum. Methods Sect. B 92, 162–165.
Mills, R.A., Elderfield, H., 1995. Hydrothermal activity and the geochemistry of metalliferous sediment. Geophys. Monogr., 91. http://dx.doi.org/10.1029/GM091p0392.
Mottl, M.J., McConachy, T.F., 1990. Chemical processes in buoyant hydrothermal plumes on the East Pacific Rise near 21°N. Geochim. Cosmochim. Acta 54, 1911–1927.
Nodder, S.D., Northcote, L., 2001. Episodic particulate fluxes at southern temperate mid-latitudes (42–45°S) in the Subtropical Front region, east of New Zealand. Deep-Sea Res. I 48, 833–864.
Palanques, A., Isla, E., Puig, P., Snaches-Cabeza, J.A., Masque, P., 2002. Annual evolution of downward particle fluxes in the Western Bransfield Strait (Antarctica) during the FRUELA project. Deep-Sea Res. II 49, 903–920.
Peter, J.M., Goodfellow, W.D., 1996. Mineralogy, bulk and rare earth element geochemistry of massive sulphide-associated hydrothermal sediments of the Brunswick Horizon, Bathurst mining camp, New Brunswick. Can. J. Earth Sci. 33, 252–283.
Proskurowski, G., Lilley, M.D., Brown, T.A., 2004. Isotopic evidence of magmatism and seawater bicarbonate removal at the endeavour hydrothermal system. Earth Planet. Sci. Lett. 225, 53–61.
Resing, J.A., Lebon, G., Baker, E.T., Lupton, J.E., Embley, R.W., Massoth, G.J., Chadwick Jr., W.W., de Ronde, C.E.J., 2007. Venting of acid-sulfate fluids in a high-sulfidation setting at NW Rota-1 submarine volcano on the Mariana Arc. Econ. Geol. 102, 1047–1061.
Stoffers, P., Worthington, T.J., Schwarz-Schampera, U., Hannington, M.D., Massoth, G.J., Hekinian, R., Schmidt, M., Lundsten, L.J., Evans, L.J., Vaiomounga, R., Kerby, T., 2006. Submarine volcanoes and high-temperature hydrothermal venting on the Tonga arc, southwest Pacific. Geology 34, 453–456.
Stoffregen, R., 1987. Genesis of acid-sulfate alteration and Au-Cu-Ag mineralization at Summitville, Colorado. Econ. Geol. 82, 1575–1591.
Taylor, S.R., McLennan, S.M., 1985. The Continental Crust: Its Composition and Evolution. Blackwell.
Walker, B.D., McCarthy, M.D., Fisher, A.T., Guilderson, T.P., 2008. Dissolved inorganic carbon isotopic composition of low-temperature axial and ridge-flank hydrothermal fluids of the Juan de Fuca Ridge. Mar. Chem. 108, 123–136.
Wedepohl, K.H., 1995. The composition of the continental crust. Geochim. Cosmochim. Acta 59, 1217–1232.
Ziegler, C.L., Murray, R.W., Hovan, S.A., Rea, D.K., 2007. Resolving eolian, volcanogenic, and authigenic components in pelagic sediment from the Pacific Ocean. Earth Planet. Sci. Lett. 254, 416–432.